T-matrix approach to quarkonium correlation functions in the quark-gluon plasma

D. Cabrera and R. Rapp

Cyclotron Institute and Physics Department, Texas A&M University, College Station, Texas 77843-3366, USA

(Received 17 November 2006; published 17 December 2007)

We study the evolution of heavy quarkonium states with temperature in a quark-gluon plasma (QGP) by evaluating the in-medium Q-$\bar{Q}$ T-matrix within a reduced Bethe-Salpeter equation in both S- and P-wave channels. The underlying interaction kernel is extracted from recent finite-temperature QCD lattice calculations of the singlet free energy of a Q-$\bar{Q}$ pair. The bound states are found to gradually move above the Q-$\bar{Q}$ threshold after which they rapidly dissolve in the hot system. The T-matrix approach is particularly suited to investigate these mechanisms as it provides a unified treatment of bound and scattering states including threshold effects and the transition to the (perturbative) continuum. We apply the T-matrix to calculate Q-$\bar{Q}$ spectral functions as well as pertinent Euclidean-time correlation functions which are compared to results from lattice QCD. A detailed analysis reveals large sensitivities to the interplay of bound and scattering states, to temperature-dependent threshold energies, and to the reconstructed correlator used for normalization. We furthermore investigate the impact of finite-width effects on the single-quark propagators in the QGP as estimated from recent applications of heavy-quark rescattering to RHIC data.

DOI: 10.1103/PhysRevD.76.114506 PACS numbers: 25.75.Nq, 12.38.Gc, 24.85.+p, 25.75.Dw

I. INTRODUCTION

Bound states of heavy quarks (charm and bottom, $Q = c, b$) have long been recognized as valuable objects for spectroscopy in quantum chromodynamics (QCD), thereby illuminating the nature of the static quark-antiquark potential (cf. Ref. [1] for a recent comprehensive overview). This opportunity carries over when embedding quarkonia into hot and/or dense matter, providing a rich laboratory for the study of medium modifications. The latter include (Debye) color screening of the Q-$\bar{Q}$ interaction, dissociation reactions induced by constituents of the medium, and the change in thresholds caused by mass (or width) modifications of open heavy-flavor states (D and B mesons or c and b quarks). The challenge is to develop a theoretical framework that allows a comprehensive description of heavy quarkonia in the quark-gluon plasma (QGP) and their production in ultrarelativistic heavy-ion collisions.

Lattice QCD (lQCD) calculations have made substantial progress in characterizing in-medium quarkonium properties from first principles. In particular, it has been found that ground-state charmonia [2–5] and bottomonia [6] do not dissolve until significantly above the critical temperature, T_c. This finding has been qualitatively supported in model calculations based on potentials extracted from lQCD, using either a Schrödinger equation to solve the bound-state problem [7–10], or a T-matrix approach which simultaneously accounts for scattering states [11]. The survival of low-lying quarkonia above T_c, in connection with effects of color screening, parton-induced dissociation and medium modified open-charm and -bottom thresholds, has recently been implemented for heavy-ion collisions [12,13].

A more quantitative (and reliable) comparison of model calculations to lQCD can be performed at the level of (spacelike) Euclidean-time correlation functions [14,15]. The latter are directly evaluated in lQCD with good accuracy, while the conversion of (timelike) spectral functions as evaluated in model approaches merely involves a straightforward convolution with a thermal weight function (as opposed to an inverse integral transform when going from Euclidean to Minkowski space). One of the challenges in such studies is that the model calculations need to describe not only the bound-state part of the spectral function but also its continuum part as well as threshold effects. In Ref. [10] a quantitative calculation of Euclidean correlators was performed using temperature-dependent heavy-quark potentials in a Schrödinger equation. The latter has been used to determine the bound-state spectrum in δ-function approximation [characterized by a binding energy and amplitude (or decay constant)], while the (onset of the) continuum was approximated with perturbation theory. While general trends of the lQCD correlators were captured, significant discrepancies were established especially in the S-wave charmonium channels (η_c and J/ψ). In particular, the importance of a reliable treatment of the continuum threshold was recognized.

In the present paper we evaluate charmonium and bottomonium correlators using a different method. The basic input are still in-medium Q-$\bar{Q}$ potentials as estimated from ($N_f = 2, 3$) lQCD, but we will employ these within a scattering equation to calculate the in-medium Q-$\bar{Q}$ T-matrix [11]. The main advantage of the T-matrix approach is that it simultaneously incorporates bound and scattering states based on the same interaction. Especially for situations of dissolving bound states (as expected for the problem at hand), the T-matrix provides a more comprehensive, and thus more reliable, description of the underlying nonperturbative effects. At the correlator level, the high-energy limit can be recovered by appropriate normalization of the uncorrelated (perturbative) limit,

and no decomposition into bound-state and continuum parts is necessary. In addition, the T-matrix equation allows for a straightforward implementation of in-medium single-particle (quark) properties via pertinent self-energy insertions in the two-particle Green's function, which we will also investigate. One has to keep in mind, however, that the applicability of the potential approach at finite temperature is not guaranteed (new scales, such as the Debye mass, may introduce, e.g., retardation effects). Therefore, one of the objectives of analyses as performed in this paper is to investigate not only how but *if* a many-body treatment based on a suitably defined heavy-quark potential can be employed for a realistic evaluation of in-medium quarkonium properties. This also raises the question of how to properly define the finite-temperature heavy-quark potential. While our calculations represent unquenched QCD, we will discuss our results in the context of lQCD correlators in quenched approximation. Such a comparison is meaningful above T_c ($T \gtrsim 1.2T_c$), where the heavy-quark free energies show little sensitivity to the flavor content of the theory ($N_f = 0, 2, 3$) when analyzed as a function of T/T_c [16].

Our article is organized as follows: in Sec. II we recall the basic setup of, and input to, the two-body scattering equation, including partial-wave expanded potentials and single-quark self-energy insertions. In Sec. III we evaluate the finite-temperature T-matrices for S- and P-wave quarkonia. We first construct heavy-quark potentials from lQCD in Sec. III A, including a discussion of its short- and long-distance limits, inherent uncertainties in its extraction, and relations to single-quark properties. This will be followed by our baseline results for the finite-temperature quarkonium T-matrices in Sec. III B. In Sec. IV the latter are first employed to construct pertinent spectral functions (Sec. IV A), followed by a calculation of Euclidean correlators (Sec. IV B) and a discussion of their properties in comparison to other model and lQCD results (Sec. IV C). Section V contains our conclusions and an outlook.

II. SCATTERING EQUATION AND IDENTIFICATION OF BOUND STATES

In this section we summarize the main features of the T-matrix approach to study quark-antiquark interactions in the QGP, as employed in Ref. [11]. It utilizes a three-dimensional reduction of the Bethe-Salpeter equation which neglects virtual particle-antiparticle loops and amounts to resumming the scattering series in ladder approximation. The pertinent Lippmann-Schwinger equation for the off-shell T-matrix in a given partial-wave channel (specified by angular momentum l) reads [17]

$$T_l(E;q',q) = V_l(q',q) + \frac{2}{\pi}\int_0^\infty dk\, k^2 V_l(q',k) G_{\bar{Q}Q}(E;k) \times T_l(E;k,q)[1-2f^Q(\omega_k)], \quad (1)$$

where q (q') are the incoming (outgoing) relative quark three-momenta in the center of mass (CM) frame and E is the CM energy [18]. Equation (1) is written for vanishing total 3-momentum of the heavy-quark pair, which gives the above (simple) form of the Pauli blocking factor with $f^Q(\omega) = [\exp(\omega/T)+1]^{-1}$. The intermediate two-particle propagator is evaluated in the Blankenbecler-Sugar (BbS) reduction scheme [19] (uncertainties due to other reduction schemes have been checked to be small [11]),

$$G_{\bar{Q}Q}(E;k) = \frac{m^2}{\omega_k}\frac{1}{s/4-\omega_k^2-2i\omega_k\,\mathrm{Im}\Sigma(\omega_k,k)}, \quad (2)$$

where ω_k is the solution of the quark dispersion relation,

$$\omega_k = \sqrt{m^2+k^2} + \mathrm{Re}\Sigma(\omega_k,k), \quad (3)$$

with a quark-mass term (m) and self-energy (Σ) to be discussed below. The interaction kernel of the scattering equation, $V_l(q',q)$, is provided by the heavy-quark potential in momentum space. It follows from a Fourier transformation of the coordinate-space potential, $V(r)$, which we obtain from lQCD calculations as elaborated in Sec. III A below. The components of the potential in the partial-wave basis are given by

$$V_l(q',q) = \frac{1}{8\pi}\int_{-1}^{+1} du_{q'q} V(\vec{q}',\vec{q}) P_l(u_{q'q}) = \frac{1}{8\pi}\int_{-1}^{+1} du_{q'q} P_l(u_{q'q}) \int d^3r V(r) e^{i(\vec{q}-\vec{q}')\vec{r}}, \quad (4)$$

with $P_l(x)$ the Legendre polynomial of degree l and $u_{q'q} = \cos\angle(\vec{q},\vec{q}')$.

The T-matrix equation (1) is solved with the algorithm of Haftel and Tabakin [20]: after discretizing the momentum integration, Eq. (1) is converted into a matrix equation,

$$\sum_{k=1}^{N} \mathcal{F}(E)_{ik} T(E)_{kj} = V_{ij}, \quad (5)$$

where, schematically, $\mathcal{F} = 1 - wVG_{\bar{Q}Q}[1-2f^Q]$ (with w denoting the integration weight). The solution for the T-matrix then follows from matrix inversion.

To assess the presence of heavy quark-antiquark bound states, the T-matrix has to be studied below the Q-$\bar{Q}$ threshold, $E_{\mathrm{th}} = 2\omega_{q=0}$. The nonrelativistic potential, $V_l(q',q)$, is only defined for real external three-momenta, and therefore an evaluation of T below the Q-$\bar{Q}$ threshold requires a prescription for the subthreshold continuation of the potential. For S-wave scattering, we follow the standard convention of setting the momenta to zero [21],

$$T_0(E < E_{\mathrm{th}}) = T_0(E; q' = q = 0). \quad (6)$$

The reliability of this continuation can be checked by exploiting the (numerical) matrix form of the scattering equation. Since a bound state corresponds to a pole of the

amplitude on the real energy axis below threshold, it follows that the determinant of the transition matrix $\mathcal{F}$ must vanish at the bound-state energy [20],

$$\det \mathcal{F}(E) = 0, \qquad E < E_{\rm th}. \tag{7}$$

A similar condition arises from the solution of the Schrödinger equation for the bound-state problem [20,22]. This is equivalent to finding the zeros of the Jost function in scattering (S-matrix) theory. For P-wave states, the potential is proportional to the ingoing and outgoing quark momentum and therefore the continuation in Eq. (6) cannot be applied. However, the condition Eq. (7) remains valid and will be used to determine P-wave bound states [23].

The quark self-energy figuring into the two-particle propagator, Eq. (2), receives contributions from interactions with (light) antiquarks and gluons in the heat bath. In Ref. [11] this was schematically written as

$$\Sigma = \tilde{\Sigma} + \int f^q T_{Qq} S_q, \tag{8}$$

where $\tilde{\Sigma}$ denotes the gluonic piece and the second term involves the heavy-light quark T-matrix closed by a light-quark propagator, S_q, and a thermal distribution, f^q. Rather than using an explicit model calculation for T_{Qq} [24], in the present work we constrain ourselves to the following levels of approximation: (a) a fixed heavy-quark mass m (i.e., $\mathrm{Re}\Sigma = 0$) together with a small imaginary part, $\mathrm{Im}\Sigma = -0.01$ GeV, mostly for numerical purposes (to avoid δ-function like bound states in the T-matrix); (b) a temperature-dependent heavy-quark mass as estimated from the asymptotic value of the lQCD heavy-quark internal energies; (c) a heavy-quark width as calculated in an effective model for resonance (plus perturbative gluon) interactions in the QGP [25], which has been shown to give reasonable agreement with data on suppression and elliptic flow of semileptonic electron spectra from heavy-quark decays in Au-Au collisions at RHIC [26]. We also note that interactions with heavy antiquarks from the medium can be safely neglected due to the smallness of the number of Q's in the system. This is different to (and simpler than) the situation of the light-quark self-energy which, in turn, figures into the calculation of the T-matrix, constituting a self-consistency problem as has been evaluated, e.g., in Ref. [11].

III. TEMPERATURE EVOLUTION OF HEAVY QUARKONIUM T-MATRICES

A. Quark-antiquark potential from lattice QCD

For the driving kernel of the scattering equation we focus on heavy-quark potentials from lQCD. There is an ongoing discussion how to properly extract them from the (static) heavy-quark free energy (which is the quantity computed in lQCD). The use of the free energy as a potential leads to a dissociation temperature of ground-state charmonia of about $T_{\rm diss} \simeq 1.1 T_c$ [27], while the lattice analysis of spectral functions suggests that η_c and J/ψ survive up to around $2T_c$. These higher values for $T_{\rm diss}$ can be recovered if the (color-singlet) internal energy,

$$U_1 = F_1 - T \frac{dF_1}{dT}, \tag{9}$$

is identified with the Q-$\bar{Q}$ potential [8–11]. Another possibility, namely, a certain linear combination of U_1 and F_1, has been suggested in Ref. [8]. The temperature derivative of discrete lQCD "data points" involved in the extraction of U_1 induces significant uncertainty which is comparable to, e.g., the difference between quenched and unquenched results (after rescaling of the critical temperature), as studied in Ref. [11]. In view of this situation, one presently has to accept a level of uncertainty in the potential. To adequately account for this, we adopt two versions of the internal energy, Eq. (9), as the potential: (i) based on fits to the three-flavor lQCD results for the free energy from Ref. [28], we explicitly perform the temperature derivative in Eq. (9); (ii) we directly fit the two-flavor lQCD internal energy data as extracted in the calculation of Ref. [29]. Further investigations of the impact of using different definitions of the Q-$\bar{Q}$ potential will be considered in future work.

In order to ensure the convergence of the scattering equation (1), the long-distance limit of the potential has to be normalized to zero, which is commonly done by subtracting the asymptotic value of the potential,

$$V(r,T) = U_1(r,T) - U_1^\infty(T), \tag{10}$$

with $U_1^\infty(T) \equiv U_1(r \to \infty, T)$. In Refs. [8–10,30,31], the linearity of the Schrödinger equation is exploited to trade the internal energy at infinite distance into the energy of the bound states. In Ref. [10], $U_1^\infty(T)$ is interpreted as an effective in-medium contribution to the quark mass, $\Delta m_Q(T) = U_1^\infty(T)/2$ and implemented as a change in the Q-$\bar{Q}$ threshold energy, $E_{\rm th} = 2m_Q + U_1^\infty(T)$, in the calculation of the mesonic spectral function. It is argued that this correction should not modify the mass operator in the Schrödinger equation since quarks inside a bound state do not "sense" the medium and therefore should not be subject to medium-induced mass modifications. This ambiguity in the interpretation of the internal energy at infinite distance can be resolved within the many-body scattering equation approach. The interaction of the quark with the surrounding medium induces a self-energy which is encoded in an effective mass change ($\Delta m_Q = \mathrm{Re}\Sigma$). As such, this medium effect has to be included in the two-particle propagator, Eq. (2), and therefore contributes in a nonlinear way as it is iterated to all orders in the scattering equation series. As we discuss in the following sections, this not only modifies the Q-$\bar{Q}$ threshold energy but the evolution of the binding energy (total mass of the bound

state) with temperature, leading to different dissociation temperatures when the effective in-medium mass is considered. In principle, the subtraction constant of the potential should vanish at short distances as to recover the perturbative normalization. This would require additional information (or assumptions) on the r-dependence which we do not consider in the present work. The calculated binding effects (and associated dissociation temperatures of the quarkonia) should therefore be considered as an upper limit. In addition, we have checked the subtraction procedure for the vacuum case: starting from the $T = 0$ Cornell potential, a typical string breaking scale of $r_{sb} \simeq 1.2$–1.4 fm [16,32] translates into a subtraction constant of $V_{sb} \simeq 1$–1.2 GeV; employing the correspondingly subtracted potential in the Lippmann-Schwinger equation (1), together with heavy-quark masses $m_{c(b)} = m^0_{c(b)} + V_{sb}/2$ and $m^0_{c(b)} = 1.32(4.73)$ GeV, we recover the correct (empirical) J/ψ (Υ) and ψ' (Υ') masses.

In line with neglecting the r-dependence in the subtraction constant for the potential, we do not consider possible momentum dependencies of the in-medium quark mass (or self-energy). Instead, we will consider two limiting scenarios, namely, (a) no in-medium mass correction and (b) in-medium effective mass as given by $\Delta m_Q(T) = U_1^\infty(T)/2$.

Finally, for the potentials in momentum space we introduce a relativistic correction motivated by the velocity-velocity (Breit) interaction in electrodynamics [33], see also Ref. [11]. It amounts to the following factor:

$$V(q', q) \rightarrow V(q', q)[1 + q'^2/\omega_{q'}^2]^{1/2}[1 + q^2/\omega_q^2]^{1/2}. \tag{11}$$

The two potentials used in this work are summarized in Fig. 1. For case (i) discussed above (extraction from the 3-flavor lQCD free energy), it evolves rather smoothly with temperature (left panel), while for case (ii) (2-flavor lQCD internal energy) the potential is initially more attractive (especially at intermediate distances, $r \simeq 0.4$ fm), but weakens rapidly with temperature (right panel) for $T \lesssim 1.5T_c$ and slows down thereafter. The rapid decrease is mostly induced by $U_1^\infty(T)$, which, at the maximum (for $T \simeq T_c$) is almost $\sim$1 GeV larger in Ref. [29] (cf. Fig. 4 therein) than in Ref. [28] (cf. Fig. 7 therein); on the other hand, above $T \simeq 1.2T_c$, $U_1^\infty(T)$ is around 0.5 GeV in both computations, and the extracted potentials in Fig. 1 agree reasonably well (as further discussed in Ref. [29], the uncertainties due to the actual light-quark masses used in the two computations are assessed to be small). Unless otherwise mentioned, our calculations below are based on the potential extracted from F_1 in Ref. [28] (left panel in Fig. 1).

B. Quarkonium T-matrices in the QGP

We now turn to the numerical results for the finite-temperature T-matrices in the c-$\bar{c}$ and b-$\bar{b}$ sectors, obtained by solving the scattering equation (1) in both S- and P-wave channels as described above.

1. S-wave states

In a first step, we consider the case of narrow quark spectral functions with $\mathrm{Im}\Sigma = -10$ MeV (for numerical purposes) and constant (temperature-independent) heavy-quark masses ($\mathrm{Re}\Sigma = 0$). The latter are fixed so that the corresponding ground states are located approximately at their vacuum masses for the lowest considered temperature ($T = 1.1T_c$), yielding $m_c = 1.7$ GeV and $m_b = 5.15$ GeV. Figure 2 summarizes the on-shell S-wave c-$\bar{c}$ scattering amplitude as a function of CM energy, for several temperatures from $1.1T_c$ to $3.3T_c$, as well as the determinant function $\det\mathcal{F}(E)$ (in arbitrary units). Since we do not include the hyperfine (spin-spin) interactions, η_c (η_b) and J/ψ (Υ) states are degenerate. At the lowest temperature, we recover the charmonium ground state at $E \approx 3.0$ GeV, and also find a cusp at the c-$\bar{c}$ threshold

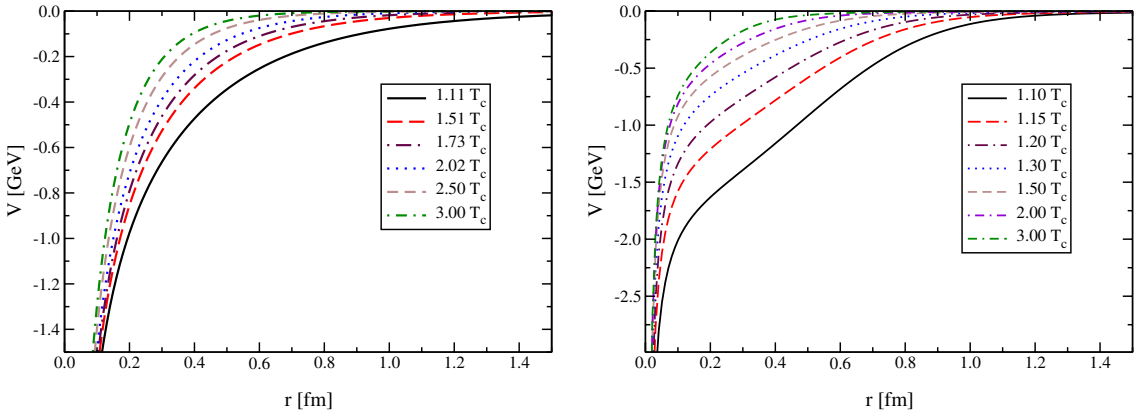

FIG. 1 (color online). Q-$\bar{Q}$ color-singlet potential for several temperatures above T_c, as defined in Eq. (10); left panel: based on F_1 from Ref. [28] ($N_f = 3$-QCD) in connection with Eq. (9); right panel: based on U_1 as numerically evaluated from $N_f = 2$-QCD results in Ref. [29]. Note the different energy scales on the two graphs.

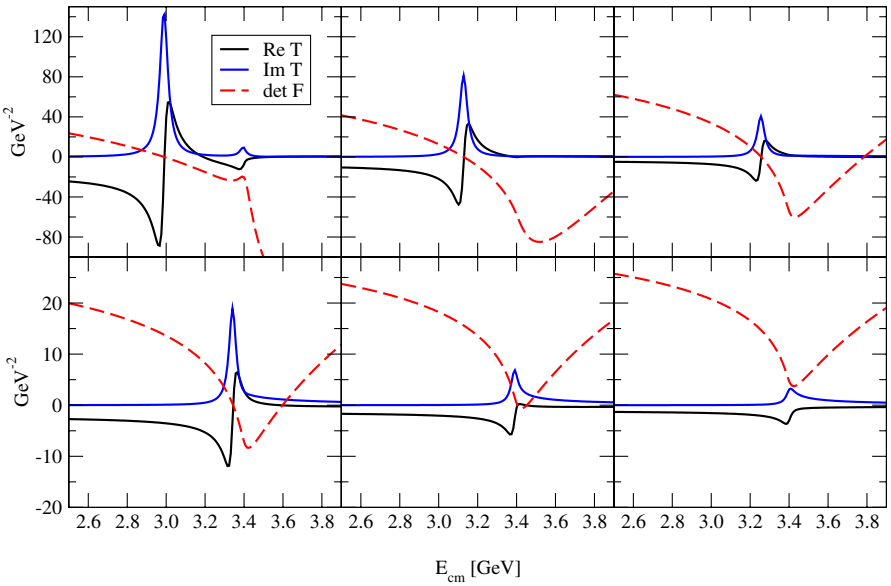

FIG. 2 (color online). Real and imaginary parts of the T-matrix for S-wave c-$\bar{c}$ scattering in the QGP based on potentials derived from the lQCD free energy of Ref. [28]. Also shown is the determinant function $\det\mathcal{F}$ (dashed line, arbitrary units). From left to right and up to down, the temperatures are $(1.1, 1.5, 2.0, 2.5, 3.0, 3.3)T_c$.

energy indicating that the first-excited state (ascribed to the ψ') has just melted. The determinant function, $\det\mathcal{F}(E)$, vanishes exactly at the ground-state energy coinciding with $\mathrm{Re}T(E) = 0$, thus corroborating our subthreshold continuation of the T-matrix, Eq. (6). For higher energies $\det\mathcal{F}(E)$ approaches zero again, but as soon as the threshold is reached it deviates indicating that the first excited state has already crossed into the continuum spectrum [34]. As the temperature is increased, the bound charmonium state gradually moves toward threshold, indicating a reduction of its binding energy. At the same time, the magnitude of the T-matrix is appreciably reduced. The $J/\psi(1S)$ survives as a bound state well beyond T_c, eventually crossing the threshold at about $(2.8–3.0)T_c$, after which it turns into a resonance and rapidly melts in the hot system [35]. Our results agree reasonably well with those of Ref. [11], with some differences in size and shape of the scattering amplitude, in particular, a larger dissociation temperature. This is mostly due to a different parametrization of the Q-$\bar{Q}$ potential (reflecting the uncertainties in a derivation

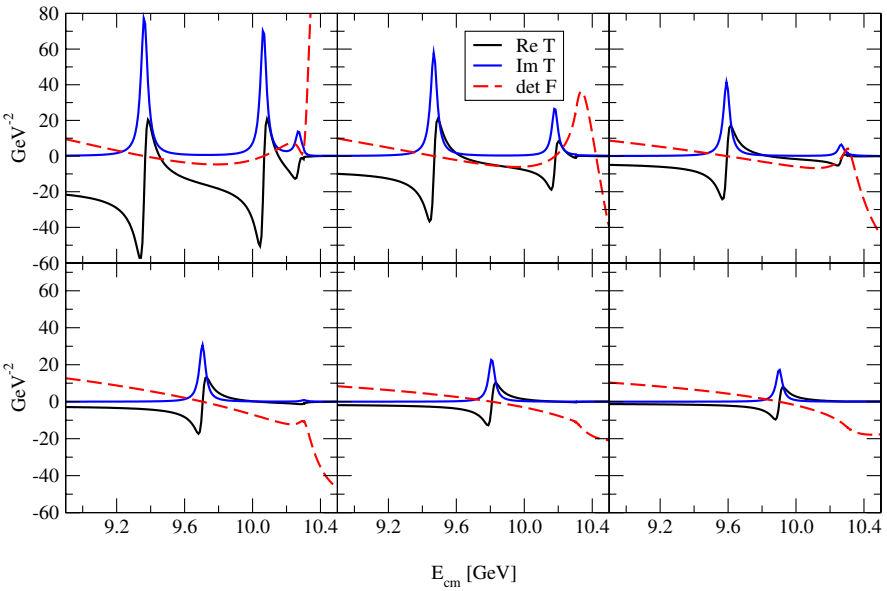

FIG. 3 (color online). Same as in Fig. 2 but for S-wave b-$\bar{b}$ scattering. From left to right and up to down, the temperatures are $(1.1, 1.5, 1.8, 2.1, 2.7, 3.5)T_c$.

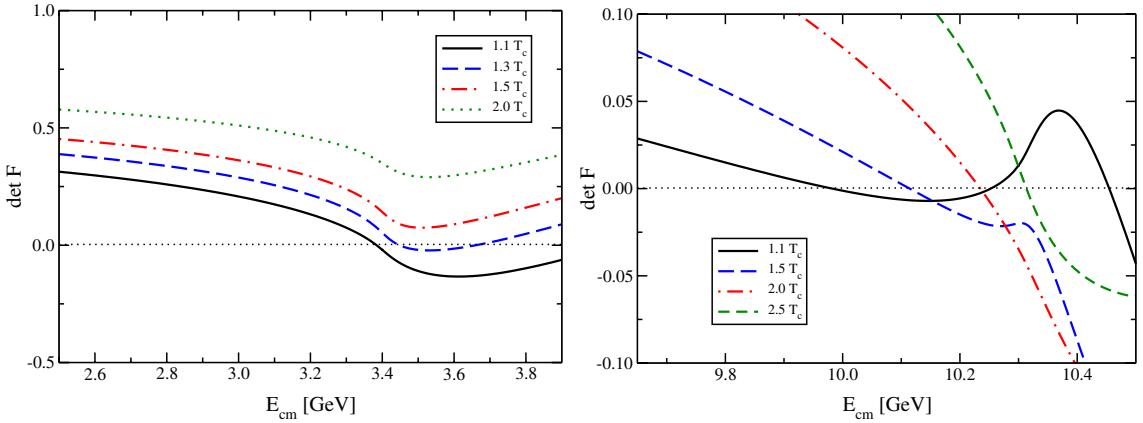

FIG. 4 (color online). Pole identification function ($\det\mathcal{F}$) for charmonium (left) and bottomonium (right) P-wave scattering at several temperatures.

of the Q-$\bar{Q}$ internal energy from a fit to the free energy, cf. Sec. III B 4 below) and a different choice of the two-particle propagator, which implies deviations at order $\mathcal{O}(p/m)$. The robustness of this approach to dynamically generate quarkonium bound and scattering states and their evolution with temperature is confirmed and extended in the following to study other quarkonium states.

The results for S-wave b-$\bar{b}$ scattering are depicted in Fig. 3. At the lowest temperature the T-matrix exhibits two bound states, as well as the remnant of a third one. The bound-state locations are again quantitatively confirmed by the vanishing determinant of the transition matrix (dashed lines), while it barely reaches zero at the location of the third structure in the T-matrix, which carries much smaller strength, indicating that it has practically melted in the medium. The two bound states at $E \approx 9.35$, 10.05 GeV are ascribed to the ground and first-excited bottomonium states $\Upsilon(1S)$, η_b and $\Upsilon(2S)$, η_b', respectively. The $\Upsilon(2S)$ moves above the b-$\bar{b}$ threshold at $T \approx 1.8T_c$, whereas the $1S$ state survives in the QGP until much higher temperatures, beyond $T \approx 3.5T_c$.

2. P-wave states

Next we study Q-$\bar{Q}$ scattering in a relative P-wave. In order to assess the formation of bound states in this channel we rely on the condition in Eq. (7) and determine the zeros of $\det\mathcal{F}(E)$, which is plotted in Fig. 4 for several temperatures for both charm and bottom. We only find one c-$\bar{c}$ bound state at the lowest temperature ($T = 1.1T_c$), at $E \approx 3.4$ GeV (just below threshold), which we associate with the $1P$ charmonium, χ_c. As the temperature increases, the χ_c state rapidly shifts into the continuum.

The P-wave b-$\bar{b}$ system exhibits two bound states at the lowest temperature, which we may identify with the $\chi_b(1P)$ and $\chi_b(2P)$ as their energies ($E = 9.95$, 10.25 GeV) are close to the nominal values in the vacuum. The $\chi_b(2P)$ state moves beyond threshold for $T \approx 1.3T_c$ and the $\chi_b(1P)$ for $T \approx 2.3T_c$. Both the mass and the binding energies, ($E_B = E_{\rm th} - M$), of the S- and P-wave states are summarized in Tables I and II for several temperatures.

3. Continuum scattering

The T-matrix approach also encompasses the continuum part of the spectrum. This is not easily appreciated in Figs. 2 and 3 because of the different scales of the narrow

TABLE I. Summary of masses and binding energies (in [GeV]) for S-wave quarkonia in the QGP as extracted from the finite-temperature T-matrix determinant, Eq. (7).

T/T_c	1.1	1.5	2.0	2.5	3.0	3.3
$M[J/\psi, \eta_c]$	2.99	3.13	3.25	3.34	≈3.40	···
$E_B[J/\psi, \eta_c]$	0.41	0.27	0.15	0.06	≈0	···
$M[\psi(2S)]$	≈3.40	···	···	···	···	···
$E_B[\psi(2S)]$	≈0	···	···	···	···	···

T/T_c	1.1	1.5	1.8	2.1	2.7	3.5
$M[\Upsilon, \eta_b]$	9.35	9.47	9.59	9.70	9.81	9.86
$E_B[\Upsilon, \eta_b]$	0.95	0.83	0.71	0.60	0.49	0.44
$M[\Upsilon(2S)]$	10.05	10.18	10.28	···	···	···
$E_B[\Upsilon(2S)]$	0.25	0.12	≈0	···	···	···
$M[\Upsilon(3S)]$	≈10.30	···	···	···	···	···
$E_B[\Upsilon(3S)]$	≈0	···	···	···	···	···

TABLE II. Same as in Table I for P-wave quarkonia.

T/T_c	1.1	1.3	1.5	2	2.3
$M[\chi_c(1P)]$	3.38	···	···	···	···
$E_B[\chi_c(1P)]$	≈0	···	···	···	···
$M[\chi_b(1P)]$	9.95	10.05	10.11	10.23	10.30
$E_B[\chi_b(1P)]$	0.35	0.25	0.19	0.07	≈0
$M[\chi_b(2P)]$	10.25	10.30	···	···	···
$E_B[\chi_b(2P)]$	0.05	≈0	···	···	···

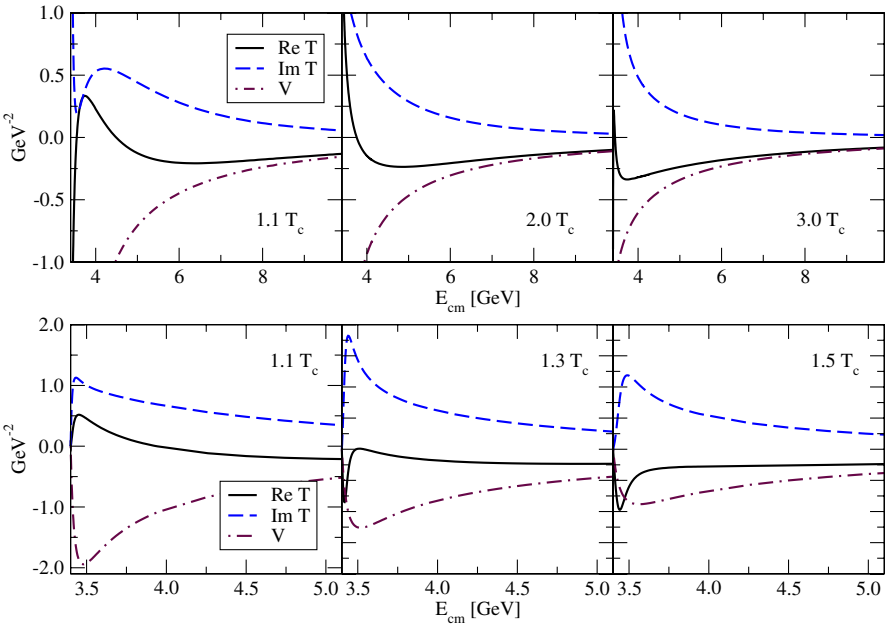

FIG. 5 (color online). c-$\bar{c}$ scattering amplitude in S- (up) and P-wave (below) above threshold. The Born approximation to the amplitude is also shown (dash-dotted).

bound-state signal and the amplitude above threshold. Note that the determinant of the transition matrix, $\det\mathcal{F}$, vanishes for some energies above threshold (cf. Figs. 2–4), possibly indicating resonant scattering in the continuum. Indeed, as can be seen in Fig. 5, the T-matrix for c-$\bar{c}$ S- and P-wave scattering exhibits substantial correlations above threshold. The imaginary part shows a distorted resonant shape, which peaks at approximately the same energy where the real part vanishes. The nonperturbative effects of the Q-$\bar{Q}$ rescattering above threshold are evident as we compare the T-matrix to its Born approximation, V (dash-dotted line in Fig. 5). We confirm that the T-matrix shows the expected behavior at high energies, i.e., the real part converges to the Born approximation and the imaginary part tends to vanish. Finally, Fig. 6 displays the imaginary part of the S-wave scattering amplitude on a logarithmic scale over a wide energy range below and above the Q-$\bar{Q}$ threshold.

We recall that nonperturbative strength in the continuum regime of the T-matrix could play an important role for providing short thermalization times for both light and heavy quarks in the QGP phase of ultrarelativistic heavy-ion collisions, cf. Refs. [11,25,26].

4. Sensitivity to lQCD potential

In Fig. 7 we show the c-$\bar{c}$ S-wave scattering amplitude based on the potential fitted directly to the internal energy data of Ref. [29]. We have kept $m_c = 1.7$ GeV for comparison with our previous results. The T-matrix exhibits

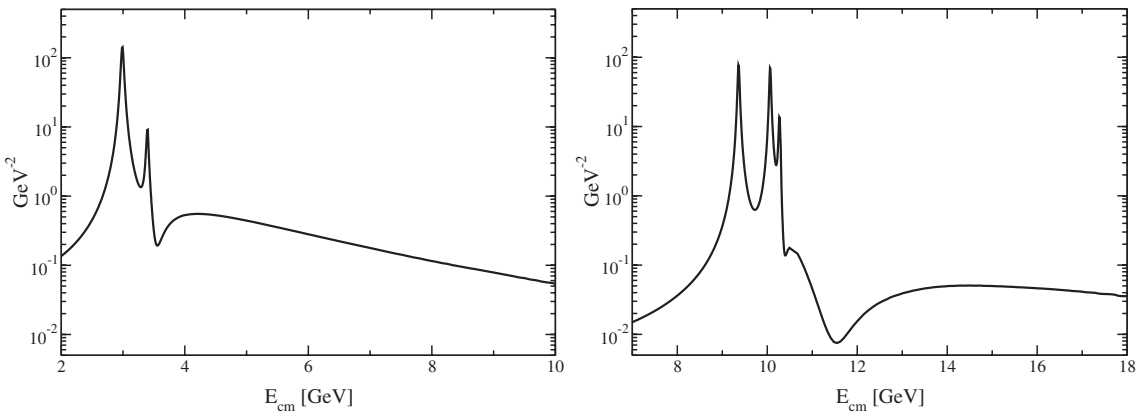

FIG. 6. Imaginary part of the S-wave scattering amplitude including bound and scattering parts of the spectrum (left: charmonium; right: bottomonium) at $T = 1.1T_c$.

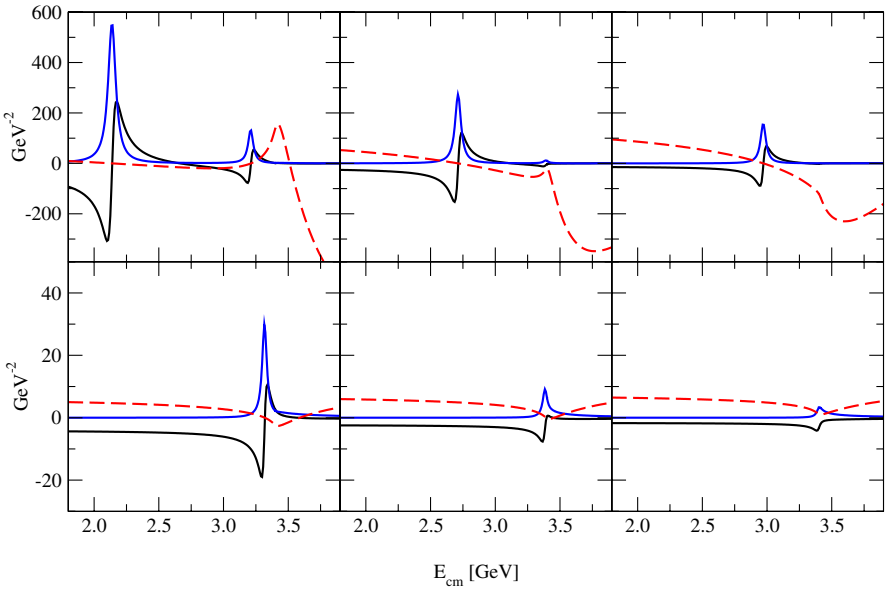

FIG. 7 (color online). Same as in Fig. 2 for the potential derived from the lQCD internal energy of Ref. [29]. From left to right and up to down, the temperatures are $(1.10, 1.15, 1.20, 1.50, 2.00, 2.50)T_c$.

two bound states with a stronger binding, as to be expected from the potential comparison in Fig. 1. With the same bare quark mass, the ground state is located at a much lower energy, $E \approx 2.2$ GeV, translating into a binding energy of about 1.2 GeV, in agreement with the results of Refs. [9,36] within a Schrödinger equation using the same potential. As the temperature increases, the bound states rapidly shift to higher energies, reflecting the rapid reduction of the potential strength at low temperatures. This trend slows down beyond $2T_c$, and the ground state eventually dissolves at $T \simeq 2.5T_c$. The large binding within this potential requires appreciable bare quark masses ($m_c \sim 2$ GeV) in order to reproduce the nominal position of the charmonium ground state in the vacuum. The strong attraction is presumably related to the entropy contribution to the Q-$\bar{Q}$ free energy at large distances (cf. Figs. 3 and 4 in Ref. [29]), which peaks at T_c and decreases steeply with temperature. The long-distance limit of the internal energy, U_1^∞, which inherits this behavior, is subtracted to generate the Q-$\bar{Q}$ potential, cf. Eq. (10). As mentioned in Sec. III A, U_1^∞ might be interpreted as a contribution to the in-medium quark mass, $m_c^*(T) = m_c + U_1^\infty(T)/2$, i.e., a quark self-energy contribution. However, if no further r-dependence (or momentum dependence) is considered, the simple subtraction of U_1^∞ from the internal energy distorts the normalization of the potential at short distances, where it should be described by perturbative QCD (one-gluon exchange). A more detailed investigation of these interplays will be carried out in future work.

5. In-medium heavy-quark masses

To end this section we present results for the c-$\bar{c}$ and b-$\bar{b}$ S-wave T-matrices when an in-medium heavy-quark mass is implemented, according to $m_Q^*(T) = m_Q + U_1^\infty(T)/2$. We readjust the corresponding bare masses so that the quarkonium ground states are located at approximately their vacuum energies for the lowest temperature considered, as in Sec. III B (namely, $m_c = 1.11$ GeV and $m_b = 4.56$ GeV). This facilitates the comparison to our results in Figs. 2 and 3, emphasizing the effect of the temperature evolution of the heavy-quark mass. Figure 8 shows the S-wave charmonium scattering amplitude, with real and imaginary parts displayed separately. The T-matrix exhibits a considerable shift to lower energies as the temperature is increased, reflecting the rather rapid decrease of $U_1^\infty(T)$ beyond T_c. Note that, while the Q-$\bar{Q}$ threshold energy is reduced, the binding energy of the bound states also decreases with increasing temperature. This compensates the downward shift of the bound states which slows down for higher temperatures. The effective quark mass not only modifies the Q-$\bar{Q}$ threshold, but also moderately changes the binding energies of the bound states since it enters the two-particle propagator in the scattering equation. Therefore, the dissociation temperatures slightly change. For example, using the bound-state condition in Eq. (7), we find $T_{\rm diss} \approx 2.5T_c$ for the charmonium ground state, as compared to $\sim 3T_c$ in the calculation with a fixed quark mass in Sec. III B 1.

The corresponding results for b-$\bar{b}$ S-wave scattering are displayed in Fig. 9. The behavior of the T-matrix is similar to the charmonium case. In particular, one observes that the bottomonium ground state is considerably shifted to lower energies as the temperature is increased. Beyond $T \approx 2.0T_c$, however, the reduction in the binding energy compensates the Q-$\bar{Q}$ threshold shift and the $\Upsilon(1S)$ state moderately evolves to higher energies.

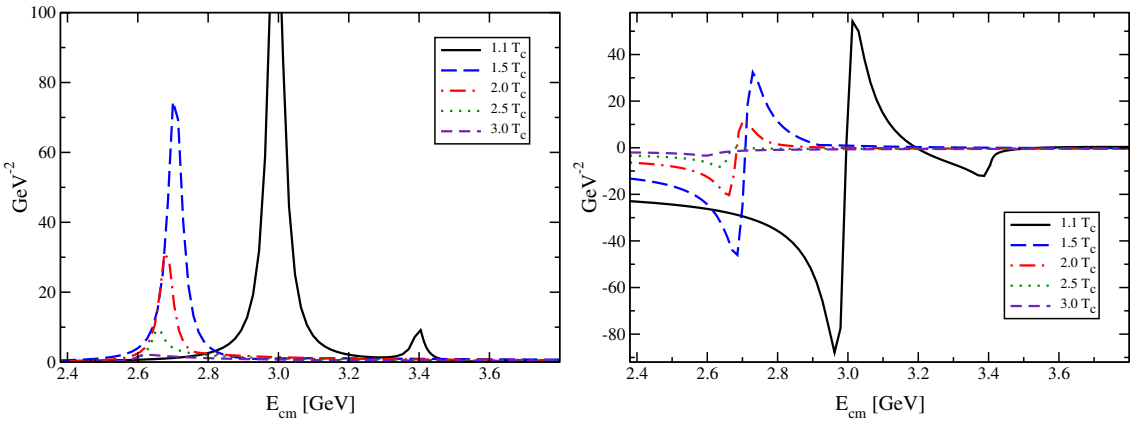

FIG. 8 (color online). Imaginary (left) and real (right) parts of the c-$\bar{c}$ S-wave scattering amplitude using an effective charm mass as explained in the text.

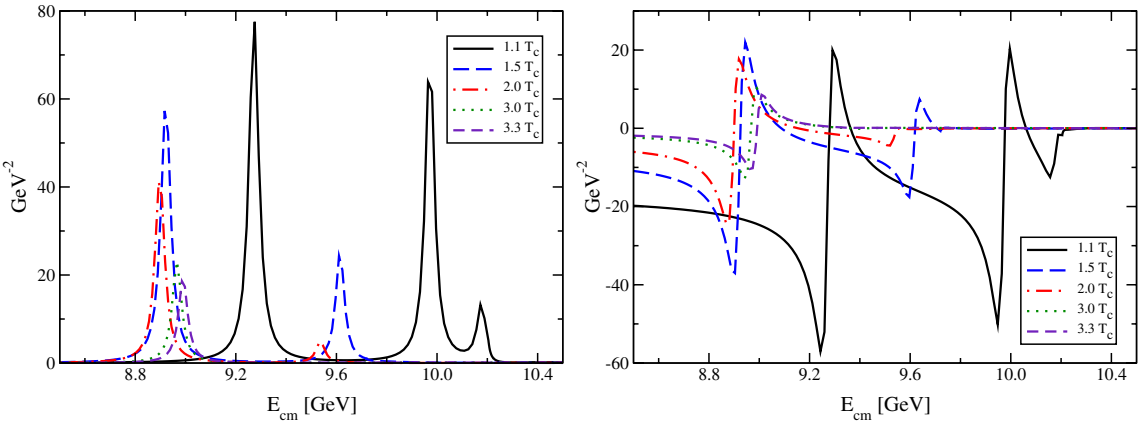

FIG. 9 (color online). Imaginary (left) and real (right) parts of the b-$\bar{b}$ S-wave scattering amplitude using an effective bottom mass as explained in the text.

IV. QUARKONIUM SPECTRAL FUNCTIONS AND EUCLIDEAN-TIME CORRELATORS

A. Spectral function

The T-matrix formalism used above can be directly applied to evaluate mesonic spectral functions for the different quarkonium channels. The spectral functions encode the information on both the bound and scattering states in the continuum ($E > E_{\rm th}$), similar to the T-matrix. Moreover, they allow for a quantitative connection between the present approach and Euclidean-time correlation functions, which have been calculated in lattice QCD with rather high precision [3,6]. Such a comparison has recently been conducted in Ref. [10] where the heavy-quark interaction in the QGP has been studied by solving the bound-state problem using a Schrödinger equation with either a screened Cornell-type potential or lQCD-based internal energies (similar to the present work). The quarkonia spectral functions were then composed of δ-function like bound states with weights determined by the decay constant of the state and a continuum assuming free quark propagation with a threshold behavior taken from perturbative QCD [37,38],

$$\sigma(\omega, T) = \sum_i 2M_i F_i^2 \delta(\omega^2 - M_i^2) + \frac{3}{8\pi^2}\omega^2 f(\omega, E_{\rm th})\Theta(\omega - E_{\rm th}). \quad (12)$$

The decay constants are related to the (derivative of the) radial wave function at the origin for S- (P-)wave states [39], while the functional form of the continuum threshold, given by $f(\omega, E_{\rm th})$, depends on the specific channel (pseudoscalar, vector, scalar, axial-vector) [37,38]. The threshold energies were set to $E_{\rm th}^{c\bar{c}} = 4.5$ GeV and $E_{\rm th}^{b\bar{b}} = 11$ GeV, based on the phenomenological observation that no narrow mesonic resonances appear in the spectrum beyond this energies. The resulting correlation functions qualitatively reproduced the features observed in lQCD for the scalar channel ($\chi_{c,b}$), whereas sizable discrepancies were found for the pseudoscalar and vector channels ($\eta_{c,b}$ and J/ψ, Υ).

In the present approach, the Q-$\bar{Q}$ system is interacting also above the Q-$\bar{Q}$ threshold with the same potential that generates the bound-state solutions, which, in particular, accounts for the transition between the discrete and the continuum part of the spectrum. To properly match the nonperturbative rescattering part of our T-matrix spectral function to the perturbative (noninteracting) term, we expand the spin structure of the former in $1/m_Q$ which allows a smooth matching between the LS classification of charmonia and the helicity representation at high energy. Nonperturbative effects play an especially important role when reduced binding energies drive states toward and across the two-particle threshold. The mesonic spectral function is given by the imaginary part of the heavy-quark two-point (current-current) correlation function in momentum space, $G(E, \vec{P})$, as pictorially represented by its perturbation series in Fig. 10. The correlation function can be calculated from the T-matrix by closing the external legs with the appropriate momentum integrations and the corresponding current operator. Schematically, one has

$$G = G^0 + G^0 T G^0, \tag{13}$$

where G^0 is the lowest order correlation function, which represents the uncorrelated Q-$\bar{Q}$ propagator in a given mesonic channel,

$$\begin{aligned} G^0(E, \vec{P} = \vec{0}; T) = i N_f N_c \int \frac{d^3k}{(2\pi)^3} \\ \times \mathrm{Tr}\{\Gamma_M \Lambda_+(\vec{k}) \Gamma_M \Lambda_-(-\vec{k})\} \\ \times G_{Q\bar{Q}}(E; k)[1 - 2 f^Q(\omega_k)], \end{aligned} \tag{14}$$

with $\Lambda_\pm(\vec{k}) = (\omega_k \gamma^0 - \vec{k}\,\vec{\gamma} \pm m_Q)/2m_Q$ the positive/negative energy projectors, $\Gamma_M = (1, \gamma_5, \gamma^\mu, \gamma^\mu\gamma_5)$ and $N_f(N_c)$ the number of flavors (colors). We take $N_f = 1, N_c = 3$ as in Ref. [10] to ensure the same normalization of the lowest order correlation function. Equation (14) denotes the finite-temperature result, and we have used the explicit decomposition of the single particle propagator, S_Q, in terms of energy projectors, which recovers the BbS 3D-reduction scheme used in the calculation of the T-matrix.

The Q-$\bar{Q}$ rescattering is encoded in the second (two-loop) term of Eq. (13). A proper connection has to be made between a potential description of the interaction and the relativistic invariant amplitude entering $\Delta G \equiv G^0 T G^0$

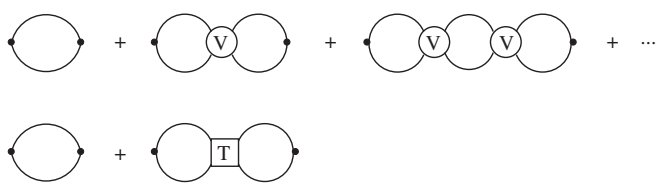

FIG. 10. Diagrammatic representation of the Q-$\bar{Q}$ correlation function. The solid dots represent Γ_M operators specifying different mesonic channels.

(see the Appendix for details). In particular, we have thus far suppressed the tensor structure of T (and V) in Dirac space. At high energies the Q-$\bar{Q}$ interaction should correspond to perturbative one-gluon exchange, which has a vector structure, whereas at low energies, according to lQCD, the potential is compatible with a scalar structure [40,41]. In the absence of further information, especially for the intermediate energy regime, we consider both tensor structures alternatively and write for the matrix elements $T_D = \bar{u}\tilde{\Gamma} u T \bar{v}\tilde{\Gamma} v$, with $\tilde{\Gamma} = 1,\ \gamma^\nu$ and $u(v)$ the positive (negative) energy Dirac spinors. This leads to the following traces to be evaluated in Eq. (13):

$$\mathrm{Tr}\,(\Gamma_M, \tilde{\Gamma}) = \mathrm{Tr}\{\Lambda_+(\vec{k}) \Gamma_M \Lambda_-(-\vec{k}) \tilde{\Gamma} \Lambda_-(-\vec{k}') \Gamma_M \Lambda_+(\vec{k}') \tilde{\Gamma}\}. \tag{15}$$

It turns out that they can be written in a partial-wave expansion as performed for the T-matrix,

$$\begin{aligned} \mathrm{Tr}\,(\Gamma_M, \tilde{\Gamma}) = a_0^{\Gamma_M, \tilde{\Gamma}}(k, k') P_0(\cos\theta_{kk'}) \\ + a_1^{\Gamma_M, \tilde{\Gamma}}(k, k') P_1(\cos\theta_{kk'}) \\ + a_2^{\Gamma_M, \tilde{\Gamma}}(k, k') P_2(\cos\theta_{kk'}), \end{aligned} \tag{16}$$

so that all angular integrations can be done analytically by using the orthogonality of the Legendre polynomials. We thus have

$$\begin{aligned} \Delta G(E; T) = N_f N_c \frac{1}{8\pi^4} \int dk\, k^2 G_{Q\bar{Q}}(E; k)[1 - 2 f^Q(\omega_k)] \\ \times \int dk'\, k'^2 G_{Q\bar{Q}}(E; k')[1 - 2 f^Q(\omega_{k'})] \\ \times \mathcal{T}(\Gamma_M, \tilde{\Gamma}; E; k, k'), \end{aligned} \tag{17}$$

with the kernel $\mathcal{T}$ given by

$$\begin{aligned} \mathcal{T}(\Gamma_M, \tilde{\Gamma}; E; k, k') \equiv \int d(\cos\theta_{kk'})\, \mathrm{Tr}(\Gamma_M, \tilde{\Gamma}; k, k', \theta_{kk'}) \\ \times T(E; \vec{k}, \vec{k}') \\ = 8\pi[a_0(k, k') T_0(E; k, k') \\ + a_1(k, k') T_1(E; k, k')], \end{aligned} \tag{18}$$

and a_l coefficients as tabulated in Table III. We note that, for a given channel, e.g. pseudoscalar, in principle both the S- and P-wave components of the T-matrix contribute to the correlation function, whereas the usual spectroscopic (nonrelativistic) characterization of quarkonium states is based on orbital angular momentum quantum numbers (LS scheme). The (undesired) mixing of S- and P-wave components in the correlation function is related to the use of the helicity basis (JM scheme) of the Q-$\bar{Q}$ spectrum at high energies, in which a different partial-wave decomposition of the T-matrix follows. However, for the scalar and pseudoscalar channels the coefficient in Table III corresponding to the ''natural'' partial wave is leading in the nonrelativ-

TABLE III. a_l coefficients in a partial-wave basis up to $L = 1$.

$\Gamma_M, \tilde{\Gamma}$	$a_0(k, k')$	$a_1(k, k')$
S,S	$\frac{k^2 k'^2}{m_Q^4}$	$-(\frac{\omega_k \omega_{k'}}{m_Q^2} + 1)\frac{kk'}{m_Q^2}$
S,V	$4\frac{k^2 k'^2}{m_Q^4}$	$2\frac{kk'}{m_Q^2}$
PS,S	$1 + \frac{\omega_k \omega_{k'}}{m_Q^2} + \frac{k^2+k'^2}{m_Q^2} + \frac{k^2 k'^2}{m_Q^4}$	$-\frac{\omega_k \omega_{k'}}{m_Q^2}\frac{kk'}{m_Q^2}$
PS,V	$-2(1 + \frac{m_Q^2 - \omega_k \omega_{k'}}{m_Q^2}) - 4(\frac{k^2+k'^2}{m_Q^2} + \frac{kk'}{m_Q^2})$	0
V,S	$3(1 + \frac{\omega_k \omega_{k'}}{m_Q^2}) + 2\frac{\omega_k \omega_{k'}}{m_Q^2} + \frac{4}{3}\frac{kk'}{m_Q^2}$	$-(2\frac{\omega_k \omega_{k'}}{m_Q^2} + 1)\frac{kk'}{m_Q^2}$
V,V	$-6 - 4\frac{k^2+k'^2}{m_Q^2} - \frac{8}{3}\frac{k^2 k'^2}{m_Q^4}$	$-4(1 + \frac{\omega_k \omega_{k'}}{m_Q^2})\frac{kk'}{m_Q^2}$
AV,S	$-1 - \frac{\omega_k \omega_{k'}}{m_Q^2} - \frac{4}{3}\frac{k^2 k'^2}{m_Q^4}$	$(2\frac{\omega_k \omega_{k'}}{m_Q^2} + 3)\frac{kk'}{m_Q^2}$
AV,V	$2(2\frac{\omega_k \omega_{k'}}{m_Q^2} - 1 - \frac{8}{3}\frac{k^2 k'^2}{m_Q^4})$	$-4\frac{\omega_k \omega_{k'}}{m_Q^2}\frac{\omega_k \omega_{k'}}{m_Q^2}$

TABLE IV. Lowest order of a_l coefficients in a $(1/m_Q)$ expansion.

$\Gamma_M, \tilde{\Gamma}$	$a_0(k, k')$	$a_1(k, k')$
S,S	$\mathcal{O}(k^2/m_Q^2)$	$-2\frac{kk'}{m_Q^2} + \mathcal{O}(k^2/m_Q^2)$
S,V	$\mathcal{O}(k^2/m_Q^2)$	$2\frac{kk'}{m_Q^2}$
PS,S	$2 + \mathcal{O}(k^2/m_Q^2)$	$\mathcal{O}(k/m_Q)$
PS,V	$-2 + \mathcal{O}(k^2/m_Q^2)$	0

istic (heavy-quark) expansion, whereas the other one, introducing an admixture of the "unnatural" partial wave, is of higher order, cf. Table IV. For simplicity, we shall work with the nonrelativistic approximation for the a_l coefficients, which filters the appropriate partial wave for the scalar and pseudoscalar channels (and for consistency with the spin-averaged nature of the interaction potential we shall consider pseudoscalar/vector, scalar/axial vector degeneracy for the correlation functions as done for the T-matrix) [42]. We comment below on the accuracy of this approximation.

B. Euclidean-time correlation functions

The Euclidean-time correlation function is defined as the thermal mesonic two-point correlation function in a mixed Euclidean-time-momentum representation [37,38,43]. It can be expressed in a spectral representation as an integral transformation of the mesonic spectral function (here $\vec{P} = \vec{0}$),

$$G(\tau, T) = \int_0^\infty d\omega \sigma(\omega, T) \mathcal{K}(\tau, \omega, T), \tag{19}$$

where the kernel of the transformation,

$$\mathcal{K}(\tau, \omega, T) = \frac{\cosh[\omega(\tau - \beta/2)]}{\sinh(\omega\beta/2)}, \tag{20}$$

is symmetric with respect to $\tau = \beta/2$ (and $\tau \in [0, \beta]$). The Euclidean-time correlation function scans the full spectrum of the system. In particular, for $\tau \to 0$ the kernel decreases rather slowly with energy and thus the correlation function is dominated by contributions of the Q-$\bar{Q}$ continuum. On the other hand, for $\tau \to \beta/2$, the kernel exhibits the maximal decrease, so that the correlation function becomes mostly sensitive to the contribution from the low-energy region of the spectrum, in particular, the bound states. To isolate the medium effects on the mesonic spectral function from the temperature dependence introduced by the kernel, it has been proposed [3,6] to normalize the correlation function at a given temperature to a so-called "reconstructed" correlation function,

$$G_r(\tau, T) = \int_0^\infty d\omega \sigma(\omega, T = 0) \mathcal{K}(\tau, \omega, T), \tag{21}$$

which is obtained by replacing $\sigma(\omega, T)$ by a reference spectral function (for instance, the vacuum spectral function), transformed with the same finite-temperature integral kernel. To facilitate the comparison to the results in Ref. [10], in Sec. IV C 1 we first adopt their choice of the reconstructed correlator by using $\sigma(\omega, T = 0)$ of the form in Eq. (12), where the coupling constants and masses for the bound-state part are extracted from a Cornell-potential based fit to the vacuum spectrum, and the shape function $f(\omega, E_{\rm th})$ is given by the perturbative QCD continuum. For the open-charm (bottom) threshold, we take $E_{\rm th}^{c\bar{c}(b\bar{b})} = 2M_{D(B)} = 3.74(10.56)$ GeV, but also check the sensitivity to changes in the pertinent free open heavy-flavor meson thresholds by using $E_{\rm th}^{c\bar{c}} = 4.5$ GeV (as in Ref. [10]) and $2m_c = 3.4$ GeV (for the fixed m_c case). As we shall see, the use of a simplified spectral function as in Eq. (12) may introduce spurious features in the normalized correlation function which could mask the actual effect of the medium-modified Q-$\bar{Q}$ interaction. To enable a more direct comparison to lQCD evaluations, in Secs. IV C 2 and IV C 3 we normalize our results to actual (vacuum) spectral functions calculated in our approach.

It is clear from Eq. (19) that the full energy regime of the spectral function figures into the calculation of the Euclidean-time correlation function. The approximations introduced in Sec. IV A are expected to be reliable including energies above the Q-$\bar{Q}$ threshold where nonperturbative effects from the Q-$\bar{Q}$ interaction prevail, as signified by the large enhancement in the T-matrix. For higher energies in the continuum region, we do not expect these approximations to hold. However, the high-energy part of the continuum is only relevant for $\tau \to 0$, where the normalized correlator approaches 1 and is no longer sensitive to the evolution of the quarkonia states with temperature.

C. Numerical results

In this section we discuss our results for the quarkonium spectral functions and correlators. Our emphasis is on a systematic illustration of how various assumptions and

effects reflect themselves in the correlators, and how these features qualitatively compare to direct evaluations of correlator ratios in lQCD. We recall that the latter are thus far restricted to quenched QCD, while our underlying heavy-quark potentials in this section pertain to $N_f = 3$ QCD. However, as discussed in the Introduction, above T_c at least a qualitative comparison should still be meaningful.

1. Constant heavy-quark mass and small width

Following our studies of the T-matrices in Sec. III B, we first investigate mesonic spectral functions and normalized correlation functions for a constant quark mass ($m_{c,b} = 1.7, 5.15$ GeV), and therefore the continuum threshold does not depend on temperature. The S-wave charmonium spectral function is shown in the left panel of Fig. 11 for several temperatures, together with the uncorrelated (perturbative) two-particle continuum, Eq. (14). As expected, the spectral function exhibits the same charmonium bound states as found in the T-matrix, as well as their evolution to higher energies as the temperature rises. At all temperatures, the (nonperturbative) rescattering of the Q-$\bar{Q}$ system dynamically generates substantial enhancement of strength above the c-$\bar{c}$ threshold relative to the uncorrelated two-particle continuum (at $T = 1.1T_c$ a remnant of the first excited state, $\psi(2S)$, is still visible). This important effect is also in line with what has been found for the T-matrix above threshold (especially when a bound state passes into the continuum).

The corresponding normalized Euclidean correlation function for the same set of temperatures is displayed in the right panel of Fig. 11. The normalized correlator converges to unity at $\tau \to 0$, which confirms the correct normalization of the continuum part of the spectrum (it is also symmetric with respect to $\beta/2$). At low τ, where the integral in Eq. (19) is mostly dominated by the continuum region, the normalized correlator moderately increases, reaches a maximum, and then flattens/drops for τ approaching $\beta/2$, indicating a loss of strength of the correlator for $T > 1.5T_c$ relative to the zero-temperature one in the low-energy part of the spectrum. The temperature evolution of the correlation function is a combined result of a decrease in binding energy of the bound states and the contribution of the nonperturbative continuum. The drop at large τ is in qualitative agreement with the lQCD charmonium S-wave correlators [3], but the latter exhibit a weaker temperature dependence (with appreciable deviations from unity only beyond $T = 1.5T_c$) and somewhat less reduction at large τ.

The charmonium spectral functions and normalized correlators for the P-wave channel are displayed in Fig. 12. As was discussed in Sec. III B, we only find a single bound state (χ_c) just below the threshold at $T = 1.1T_c$, which rapidly melts into the continuum as temperature increases. Consequently, a sizable threshold enhancement effect is observed. Despite the fast melting of the P-wave state, the normalized correlation function steeply rises in the low-τ regime, due to (i) the contribution from the nonperturbative rescattering above threshold, and (ii) a larger threshold energy in the schematic vacuum spectral function entering the reconstructed correlator. For $\tau \to \beta/2$, the correlator stays well above unity, due to the absence of an energy gap between the P-wave state and the continuum, which renders the (enhanced) continuum contribution to the correlator dominant even for $\tau \to \beta/2$. The main features of our results at a given temperature are qualitatively in line with the lQCD P-wave correlators [3]; however, the temperature dependence is not: our correlators attenuate with temperature whereas the lQCD correlators increase. This appears to be a rather direct indication that the in-medium c-$\bar{c}$ threshold is lowered with increasing temperature.

While our results are qualitatively similar to those of Ref. [10], the following observations are in order. In Ref. [10], the increase of the correlator at low and inter-

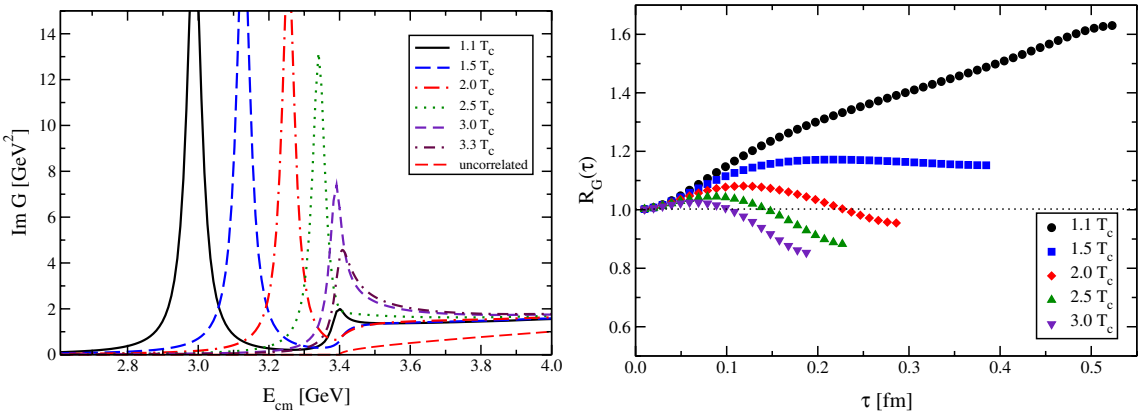

FIG. 11 (color online). Left panel: Imaginary part of the correlated two-particle propagator (Green's function) for c-$\bar{c}$ S-wave scattering at several temperatures and constant quark mass, $m_c = 1.7$ GeV. The imaginary part of the uncorrelated propagator (dashed line) is also shown for reference. Right panel: Corresponding normalized mesonic correlation functions [using Eq. (12) as the reconstructed correlator].

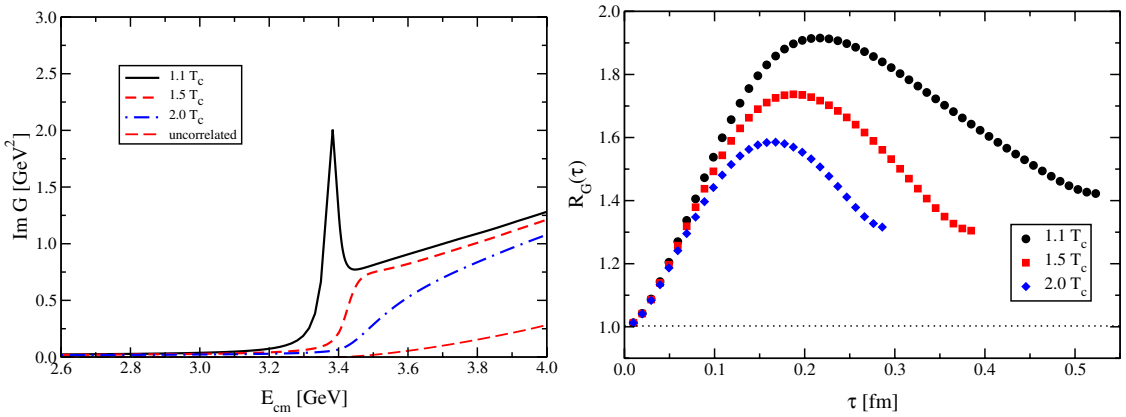

FIG. 12 (color online). Same as in Fig. 11 for c-$\bar{c}$ P-wave scattering.

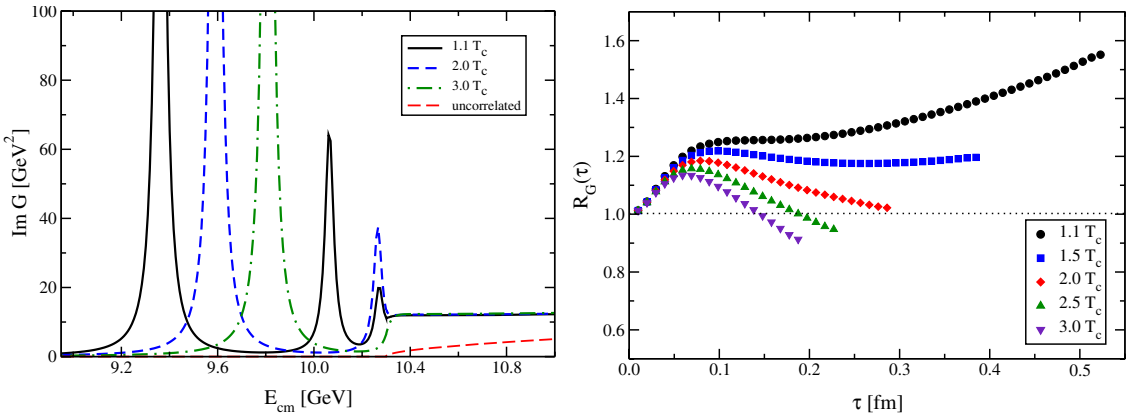

FIG. 13 (color online). Same as in Fig. 11 for b-$\bar{b}$ S-wave scattering.

mediate τ is induced by the temperature-dependent decrease of the continuum threshold. Thus far, we have not considered the temperature effect on the Q-$\bar{Q}$ threshold. However, the nonperturbative enhancement in the spectral function around threshold and above, which is not included in Ref. [10], turns out to be essential for a quantitative assessment of the quarkonium correlation (and spectral) functions, especially when the energy gap between the discrete and continuum parts of the spectrum is small or absent [30,44,45]. Nevertheless, our results leave room for a lowering of the Q-$\bar{Q}$ threshold energy, since a downward shift of strength in the spectral function would improve (i) on the large-τ decrease in the S-wave correlator, and (ii) on the temperature dependence in the P-wave correlator, as discussed below.

The bottomonium spectral and correlation functions follow a similar pattern as for the charmonium system. The results for S-wave scattering are displayed in Fig. 13. At large Euclidean time, the correlator decreases with temperature as the two excited bottomonia disappear into the continuum. Despite the survival of the $\Upsilon(1S)$ state up to rather high temperatures, the correlator looks rather similar to the charmonium case. We find slightly more enhancement at low τ, partly due to the continuum enhancement over the zero-temperature case which becomes more relevant as the bound-state binding energies decrease with temperature.

The P-wave bottomonium correlator, Fig. 14, shows a large enhancement at all τ, even larger than that of the P-wave charmonium correlator. A similar enhancement is observed in the scalar bottomonium correlator from lQCD [6]. As the temperature increases, the two bound states gradually move to higher energies and the correlator is notably attenuated. Again, as the ground state approaches the continuum the nonperturbative threshold strength in the spectral function is the decisive source of the remaining correlator enhancement. This reiterates the point that a comprehensive description of the Euclidean-time correlators should account for both the bound-state properties and Q-$\bar{Q}$ correlations above threshold.

2. Sensitivity to the reconstructed correlator

Although our results thus far reproduce some of the trends of the normalized correlators from lQCD, the S-wave correlator exhibits a τ dependence which is inconsistent with lQCD results especially for $T < 2T_c$ where the

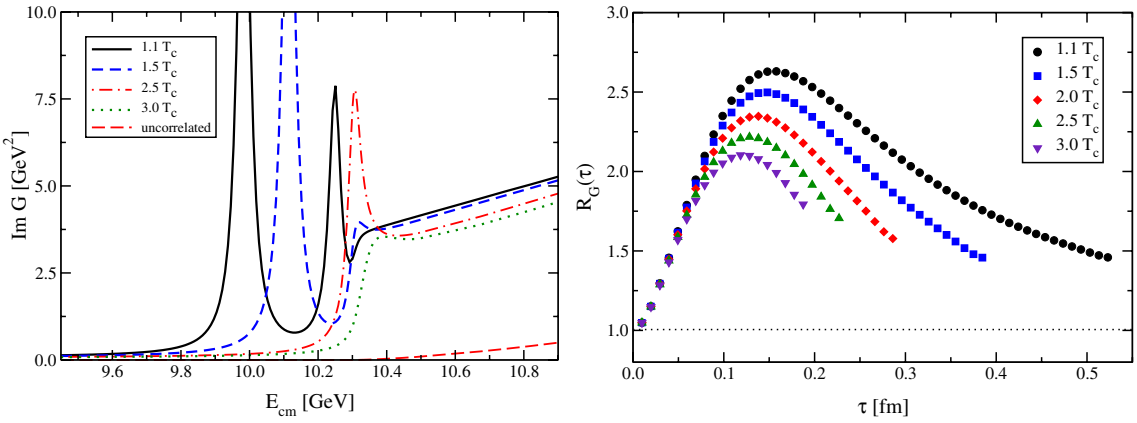

FIG. 14 (color online). Same as in Fig. 11 for b-$\bar{b}$ P-wave scattering.

increase in the low- and intermediate-τ regime is at variance with the lQCD correlators which are essentially unmodified. As discussed above, one reason for this rise is the threshold mismatch between the finite-temperature spectral function and the vacuum one, which is modeled according to Eq. (12). We therefore investigate alternative inputs for the reconstructed correlator used for normalization.

First, we vary the continuum energy threshold of the vacuum spectral function, Eq. (12), in the range $E_{\rm th}^{c\bar{c}} = 3.4$–$4.5$ GeV. The pertinent ratios for S- and P- charmonium correlators are compared in Fig. 15 to our earlier result (right panels in Figs. 11 and 12) at the lowest temperature, $T = 1.1T_c$. Not surprisingly, the low-τ rise of both amplitudes is reduced (amplified) appreciably due to the lowered (raised) threshold energies. At large τ, the S-wave correlator changes less, as expected since the discrete (low-energy) part of the spectrum in the reference spectral function is unchanged. However, one notices comparably larger changes of the P-wave correlator at large τ, since the small binding of the χ_c makes the correlator sensitive to the continuum contribution in the entire τ domain.

Second, we employ as reconstructed correlator the one based on the zero temperature T-matrix calculated with the Cornell potential and a subtraction constant defined at the characteristic string breaking scale in vacuum as discussed in Sec. III A (the T-matrix properly reproduces the empirical bound-state spectrum). As it is shown in Fig. 16, because of an increased (nonperturbative) strength in the T-matrix-based vacuum correlator (relative to the schematic one), the correlator ratios in both S- and P-wave are reduced. For the former, the agreement with lQCD results appears to improve, while for the latter it becomes worse.

To summarize this section, we note that the correlator ratios carry significant sensitivity to the underlying reconstructed correlators used for normalization, inducing appreciable variations in the absolute magnitude and shape of the normalized correlators. In particular, we find that the appreciable enhancement above one for the S-wave corre-

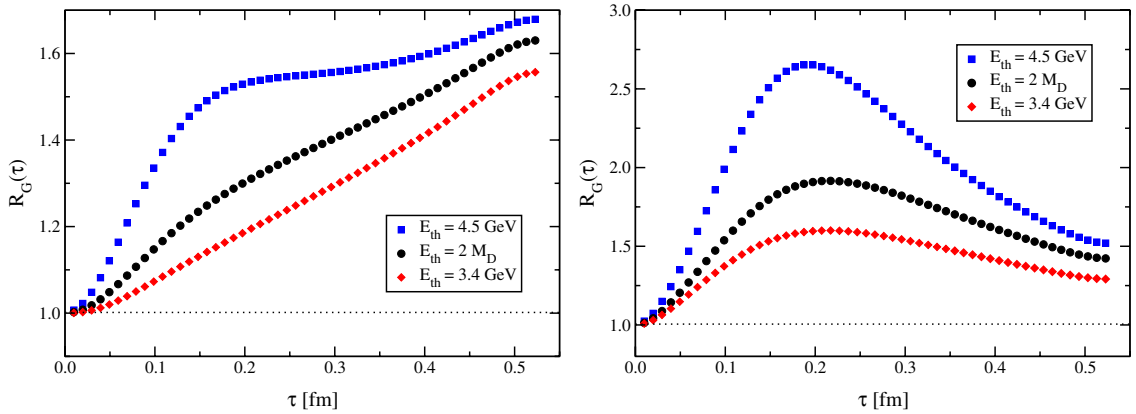

FIG. 15 (color online). Normalized correlation functions for c-$\bar{c}$ S-wave (left) and P-wave (right) scattering at $T = 1.1T_c$. As indicated in the legend, three different continuum threshold energies have been used in the zero-temperature spectral function, Eq. (12): $E_{\rm th}^{c\bar{c}} = 4.5$ GeV as in Ref. [10], the vacuum open-charm threshold, and $E_{\rm th}^{c\bar{c}} = 2m_c$ with $m_c = 1.7$ GeV.

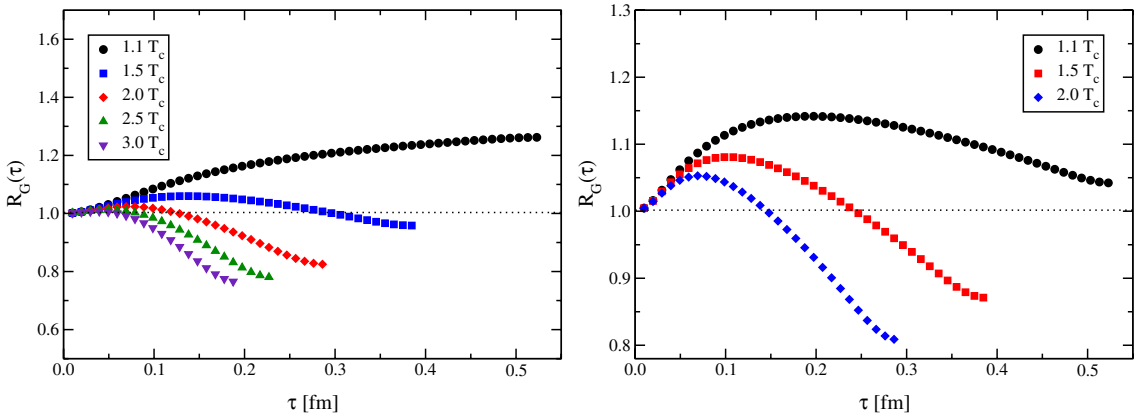

FIG. 16 (color online). Normalized correlation functions for c-$\bar{c}$ S-wave (left) and P-wave (right) scattering with a reconstructed correlator based on the vacuum T-matrix as calculated within our approach.

lators found in the previous section is in large part due to the use of a schematic reconstructed correlator. Using for the latter the vacuum correlator this feature is limited to a 20% effect. We also found that the open-charm threshold (i.e., charm-quark mass) has a significant impact on the normalized correlator. Indeed, as we will see in the next section, using an in-medium threshold as inferred from the subtraction in the internal energy, the S-wave correlator is further reduced for temperatures close to T_c, exceeding one by merely 5%.

3. In-medium heavy-quark masses and widths

We finally consider the effect of in-medium properties of the interacting charm quarks, both due to real and imaginary parts of their self-energy.

First, we incorporate an effective in-medium quark mass as extracted from the large-distance plateau of the internal energy,

$$m_c^*(T) = m_c^0 + U_1^\infty(T)/2. \tag{22}$$

We neglect a possible momentum dependence of this correction, following the discussion in Sec. III B 5. We recall that in our approach an effective heavy-quark mass not only modifies the $c\bar{c}$ threshold energy ($E_{\rm th} = 2\omega_{q=0} = 2m_c^*$), but also figures into the two-particle propagator as a self-energy contribution and is therefore iterated in the scattering equation. We implement $m_c^0 \simeq 1.3$ GeV and use $m_c = m_c^0 + V_{sb}/2 \simeq 1.9$ GeV for the vacuum calculation to properly reproduce the vacuum spectrum employing the Cornell potential with string breaking effects in the T-matrix equation, cf. Sec. III A. The pertinent vacuum spectral function will be used for the reconstructed correlator. The S-wave spectral functions are displayed in the left panel of Fig. 17. The vacuum spectral function exhibits two bound states at energies corresponding to the J/ψ and ψ', whereas the continuum opens at about 3.8 GeV ($E_{\rm th} \simeq$

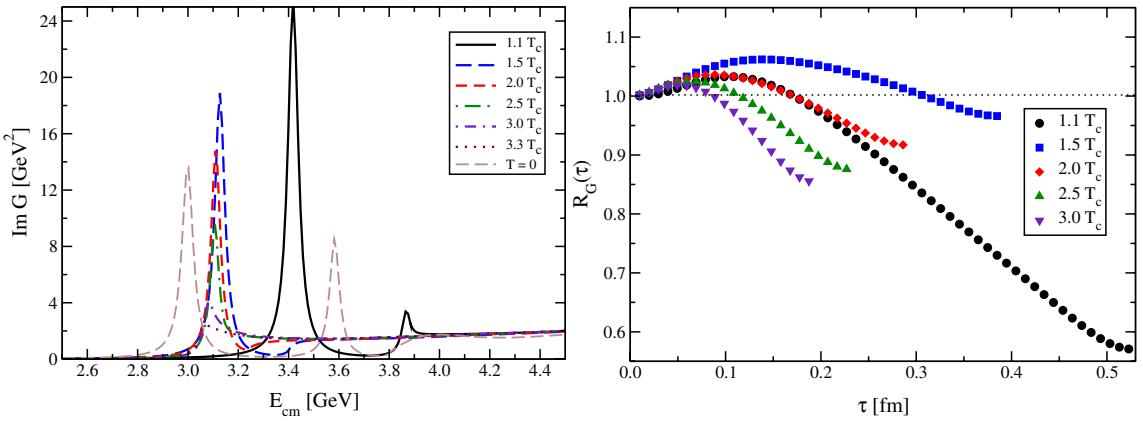

FIG. 17 (color online). Left panel: Imaginary part of the correlated two-particle propagator (Green's function) for c-$\bar{c}$ S-wave scattering at several temperatures using the effective quark mass, $m_Q^*(T)$. The zero-temperature spectral function is also shown (see the text for details). Right panel: Corresponding mesonic correlation function at several temperatures, normalized to the vacuum spectral function.

$2M_D$) and exhibits a wide resonant structure above the c-$\bar{c}$ threshold. The ground state in the in-medium spectral function is first shifted upward to $E = 3.4$ GeV at $1.1T_c$, due to a reduction in binding energy (and a slightly larger in-medium m_c^*), but shifts down to $E \simeq 3.1$ GeV when the temperature increases despite the reduction in binding, due to a larger reduction in m_c^*. The latter is also responsible for a considerable amount of continuum strength migrating to lower energies. The ground state dissolves at $T_{\rm diss} \approx 3T_c$. The resulting (normalized) S-wave correlator exhibits a (decreasing) temperature dependence that is roughly in line with the finite-T lQCD results at temperatures $T \gtrsim 1.5T_c$, with changes at the level of 10%–15%. For temperatures close to T_c, the increasing values for $U_1^\infty(T)$ induce a sizable upward shift of the bound-state mass relative to the $T = 0$ spectrum, resulting in a reduction of the correlator which is larger than found on the lattice. This suggests that the increase of $U_1^\infty(T)$ close to T_c does not (entirely) correspond to an increasing in-medium c-quark mass (but encodes, e.g., the onset of string formation). Indeed, recent lQCD analysis of charmonium properties in quenched QCD finds a temperature dependent J/ψ mass reduction of only $\sim$100 MeV at $1.3\,T_c$ [46], which is significantly smaller than the change observed in ImG from 1.1 to 1.5 T_c in the left panel of Fig. 17. For more stringent conclusions the present uncertainties in the extraction of the heavy-quark potential, as well as the assumption of a 3-momentum independent mass correction (which upsets the perturbative normalization of the potentials at short distances and therefore represents an upper estimate of the in-medium mass effect), need to be scrutinized.

For the P-wave channel (not shown), it is worth noting that the implementation of $m_c^*(T)$ improves the temperature dependence of the normalized correlator as compared to Fig. 12, even though the magnitude and time dependence are not quantitatively reproduced. Very recently it has been pointed out that the Euclidean correlator in the scalar channel receives diffusive contributions from zero-mode excitations [47] which we have not considered here. These contributions might cure the discrepancies in the P-wave channel, according to Refs. [48,49]. We shall include these contributions in a forthcoming publication.

Our analysis reconfirms the importance of a proper understanding and implementation of in-medium heavy-quark masses and threshold effects when conducting quantitative comparisons to the lQCD correlators. Further investigations of the normalization and in-medium mass issues close to T_c will be reported in future work.

Second, we address the sensitivity of the correlators to finite quarkonium widths, which constitute an essential ingredient in the phenomenology of heavy quarks and quarkonia in heavy-ion collisions. As suggested by recent analysis of heavy-quark diffusion in a QGP [25,26], as well as parton-induced breakup reactions of charmonia [12],

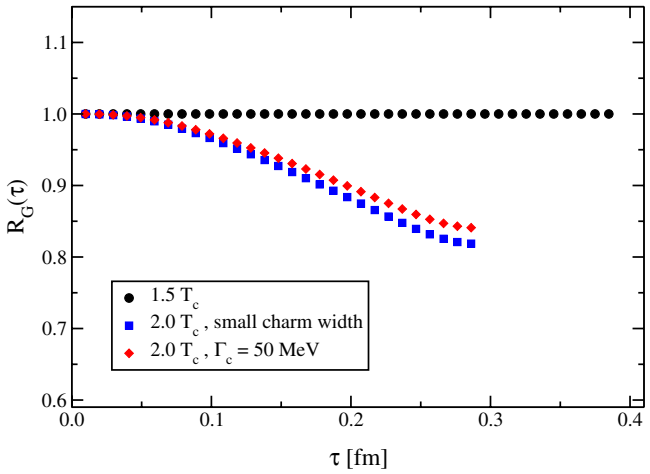

FIG. 18 (color online). S-wave charmonium correlators at $2T_c$ with a charm width of 50 MeV, as compared to the narrow quark calculation (the correlators have been normalized to the one at $1.5T_c$).

charmonium widths are expected to be of the order of 100 MeV or more at temperatures around $1.5T_c$. We can easily incorporate such effects by dressing the charm quarks with an imaginary self-energy in the two-particle propagator, Eq. (2) (for small binding energies, $E_B < T$, the width due to gluon dissociation, $g + J/\psi \to c\bar{c}$, is suppressed [50]; however, for the spectral function only the total charmonium width enters). The results for the S-wave charmonium correlation function in the fixed quark-mass scenario are indicated in Fig. 18, for a charm-quark width of 50 MeV (generating charmonium widths of $\sim$100 MeV) in comparison with the narrow-width limit (for simplicity, we have used the correlator at $1.5T_c$ as the reconstructed one). The Euclidean correlator at $2T_c$ is modified by only a few percent. Especially in view of other current uncertainties, the correlators appear rather insensitive to phenomenologically relevant magnitudes of the quarkonium decay widths; this may not be surprising since $\Gamma_\psi \simeq 0.1$ GeV is less than 5% of the charmonium mass, and also appreciably smaller than the typical QGP temperature.

V. CONCLUSIONS AND OUTLOOK

In the present article we have evaluated spectral properties of heavy quark-antiquark interactions (charm and bottom) in the quark-gluon plasma within a T-matrix approach which allows for a comprehensive treatment of bound and scattering states. The basic interaction was taken to be a two-body potential which, following earlier works, has been identified with the heavy-quark internal energy evaluated in thermal lattice QCD. The finite-temperature T-matrices confirm the previously found survival of the S-wave ground state in the QGP for temperatures up to $\sim 2.5 - 3T_c$ ($> 3.5T_c$) for $\eta_c/J/\psi$ (η_b/Υ), as

well as for excited bottomonia. The dissociation mechanism is characterized by a bound state passing through the Q-$\bar{Q}$ threshold, at which point a strong reduction and broadening of the (imaginary part of the) T-matrix occurs. Thereafter, the Q-$\bar{Q}$ system remains strongly correlated in the continuum, as indicated by resonantlike structures in the T-matrix (albeit at much reduced magnitude) which exceed the Born approximation up to energies of 1–2 GeV above the Q-$\bar{Q}$ threshold.

We have proceeded to calculate Q-$\bar{Q}$ current-current correlation functions, which, in the timelike regime, follow from the T-matrix by folding with the Q-$\bar{Q}$ propagator. The imaginary part of the correlation function (spectral function) corroborates the importance of threshold effects in the dissolution mechanisms, resulting in large (nonperturbative) enhancements over the perturbative form of the continuum. These, in turn, give substantial contributions to the Euclidean correlators primarily at large and intermediate time, τ, which cannot be neglected in quantitative analyses of lattice QCD results. Assuming constant heavy-quark masses, some qualitative features of the lQCD correlators (large-τ decrease in the S-waves, overall increase in the P-waves) can be reproduced. However, the magnitude of the signal in the S-wave channels, as well as the temperature dependence in the P-wave channels, are inconsistent with lQCD.

We have found an appreciable sensitivity of the Euclidean correlator ratios to the reference spectral function used for normalization (usually taken as a vacuum form). The choice of shape and onset of the continuum introduces τ-dependencies in the normalized correlator which can affect the interpretation of medium effects in the calculated spectral functions. To reduce uncertainties due to the normalization of the Euclidean correlators, we have calculated the spectral functions of the system at zero temperature in our scattering approach, using the Cornell form of the interaction potential with string breaking effects. The corresponding vacuum spectral functions correctly reproduce vacuum quarkonium states as well as the onset of the continuum at the open-charm (-bottom) threshold. From the evaluation of the Euclidean correlators normalized with the vacuum spectral function we have inferred that the lQCD evaluations favor a temperature-dependent decrease of the heavy-quark mass (Q-$\bar{Q}$ threshold), which pushes spectral strength to lower energies and improves on the large-τ and temperature dependence of the correlators. However, large values of the effective quark mass close to T_c, as suggested by the large-distance limit of the internal energy, entail too strong a reduction of the S-wave charmonium correlator close to T_c.

Our approach furthermore allows establishing a closer connection to quarkonium phenomenology in heavy-ion collisions by incorporating finite-width effects. For example, when implementing in-medium heavy-quark widths of ~50 MeV in the two-particle propagator of the scattering equation (inducing a charmonium width of ~100 MeV as suggested by phenomenology), we find only few-percent changes in the Euclidean correlators, which are superseded by other current uncertainties.

In conclusion, our results suggest that lQCD-based potential approaches, when consistently implementing both bound and scattering states in a nonperturbative scheme, are a valuable tool to quantitatively interpret the lQCD computations on Euclidean correlation functions, and thus evaluate the properties of quarkonium spectral functions in the QGP (supporting the notion of an ''in-medium'' heavy-quark potential). Significant uncertainties remain in the extraction of an appropriate Q-$\bar{Q}$ potential, as well as in the determination of the in-medium open-charm and -bottom masses. If quantitative agreement between model calculations and lQCD correlators can be established, applications to high-energy heavy-ion collisions will subject the theoretical results to experimental tests. Hopefully, this facilitates progress on the long-standing challenge of connecting heavy-quarkonium observables to properties of the finite-temperature QCD phase transition.

ACKNOWLEDGMENTS

We thank M. Mannarelli and F. Zantow for providing us with their (fits to) lattice QCD results. We also acknowledge useful discussions with M. Mannarelli and H. van Hees. One of us (D. C.) thanks Ministerio de Educación y Ciencia (Spain). One of us (R. R.) has been supported in part by a U.S. National Science Foundation CAREER Award under Grant No. PHY0449489.

APPENDIX: THREE-DIMENSIONAL REDUCTION OF THE BETHE-SALPETER EQUATION

The Bethe-Salpeter equation for Q-$\bar{Q}$ scattering with the BbS three-dimensional reduction of the two-particle propagator [19,51] reads, in the CM frame,

$$\mathcal{M}(E;\vec{q}',\vec{q}) = \mathcal{V}(\vec{q}',\vec{q}) + \int \frac{d^3k}{(2\pi)^3}\mathcal{V}(\vec{q}',\vec{k})\frac{m^2}{\omega_k} \times \frac{\Lambda_+(\vec{k})\Lambda_-(-\vec{k})}{s/4-\omega_k^2+i\epsilon}\mathcal{M}(E;\vec{k},\vec{q}), \tag{A1}$$

where the invariant amplitudes $\mathcal{M}$ and $\mathcal{V}$ are actually operators (truncated amplitudes) which act in the direct product of the Dirac spaces of each fermion. The BbS scheme, originally formulated for the nucleon-nucleon (NN) interaction, exploits the following decomposition of the single-particle propagator in terms of positive-energy and negative-energy states,

$$S_F(k^0,\vec{k}) = \frac{m}{\omega_k}\frac{\Lambda_+(\vec{k})}{k^0-\omega_k+i\eta} - \frac{m}{\omega_k}\frac{\Lambda_-(-\vec{k})}{k^0+\omega_k-i\eta}. \tag{A2}$$

Consequently, the full four-dimensional two-particle propagator, $iS_Q(k+P/2)S_{\bar{Q}}(k-P/2)$, is replaced by the

following function:

$$\delta(k^0)\frac{m^2}{\omega_k}\frac{\Lambda_+(\vec{k})\Lambda_-(-\vec{k})}{s/4-\omega_k^2+i\epsilon}, \tag{A3}$$

which has the same discontinuity across the right-hand cut and puts the quark (antiquark) on the positive (negative) energy shell, suppressing virtual antiquark (quark) contributions. Note that, since both fermions are equally off-shell the energy transfer at the interaction is zero (BbS neglects retardation effects), and this allows for a description in terms of a static potential, $V(\vec{q}', \vec{q})$, as done for instance in the boson exchange model of the NN interaction [51].

One can take matrix elements in Eq. (A1) between the appropriate Dirac spinors, $\tilde{T}[\tilde{V}] \equiv \bar{u}(\vec{q})\bar{v}(-\vec{q}')\mathcal{M}[\mathcal{V}]u(\vec{q}')v(-\vec{q})$ (see Fig. 19 for kinematics), and then Eq. (A1) can be rewritten as (helicity indices omitted)

$$\tilde{T}(E;\vec{q}',\vec{q}) = \tilde{V}(\vec{q}',\vec{q}) + \int\frac{d^3k}{(2\pi)^3}\tilde{V}(\vec{q}',\vec{k})\frac{m^2}{\omega_k} \times\frac{1}{s/4-\omega_k^2+i\epsilon}\tilde{T}(E;\vec{k},\vec{q}), \tag{A4}$$

where we have used the following representation of the energy projectors:

$$\Lambda_+(\vec{k}) = \frac{\sum_\lambda u_\lambda(\vec{k})\bar{u}_\lambda(\vec{k})}{2m}, \qquad \Lambda_-(\vec{k}) = \frac{-\sum_\lambda v_\lambda(-\vec{k})\bar{v}_\lambda(-\vec{k})}{2m}. \tag{A5}$$

The connection between $\tilde{T}$, $\tilde{V}$ and the actual (static) potential V and the T-matrix in Eq. (1) can be derived by considering a tensor structure for $\tilde{V}$ and performing a nonrelativistic reduction of the resulting amplitude (for instance consider $\tilde{V}$ given by the Yukawa scalar-meson exchange amplitude, which can be fully derived from the Lagrangian, $\mathcal{L}_S = g_S\bar{\Psi}\Psi\phi$). It turns out that $\tilde{V}(\vec{q}', \vec{q}) = V(\vec{q}', \vec{q}) + \mathcal{O}(q^2/m^2)$, with V related to the corresponding potential in coordinate space by

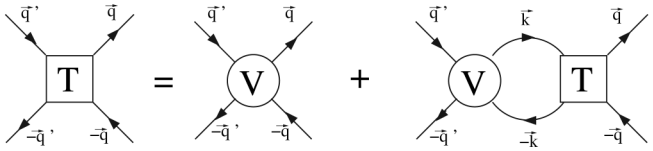

FIG. 19. CM kinematics of the Bethe-Salpeter equation.

$$V(r) = \frac{1}{(2\pi)^3}\int d^3k\, e^{i\vec{k}\vec{r}}V(\vec{k}), \tag{A6}$$

and $\vec{k} = \vec{q}' - \vec{q}$. The partial-wave decomposition of the potential (and of T) is given by

$$V(\vec{q}',\vec{q}) = 4\pi\sum_l(2l+1)V_l(q',q)P_l(\cos\theta_{q'q}), \tag{A7}$$

and then Eqs. (1) and (4) follow. The temperature dependence is accounted for by introducing a $[1-2f^Q]$ factor for each two-particle loop, and the quark self-energy enters the two-particle propagator by the replacement

$$[s/4-\omega_k^2+i\epsilon]^{-1} \to [s/4-\omega_k^2-2i\omega_k\,\mathrm{Im}\Sigma]^{-1} \tag{A8}$$

in Eq. (A4), with ω_k satisfying the dispersion relation in Eq. (3).

[1] N. Brambilla *et al.*, arXiv:hep-ph/0412158.
[2] M. Asakawa and T. Hatsuda, Phys. Rev. Lett. **92**, 012001 (2004).
[3] S. Datta, F. Karsch, P. Petreczky, and I. Wetzorke, Phys. Rev. D **69**, 094507 (2004).
[4] T. Umeda, K. Nomura, and H. Matsufuru, Eur. Phys. J. C **39S1**, 9 (2005).
[5] R. Morrin, A. P. Ó Cais, M. B. Oktay, M. J. Peardon, J. I. Skullerud, G. Aarts, and C. R. Allton, Proc. Sci., LAT2005 (2006) 176.
[6] K. Petrov, A. Jakovac, P. Petreczky, and A. Velytsky, Proc. Sci., LAT2005 (2006) 153.
[7] E. V. Shuryak and I. Zahed, Phys. Rev. C **70**, 021901 (2004).
[8] C. Y. Wong, Phys. Rev. C **72**, 034906 (2005).
[9] W. M. Alberico, A. Beraudo, A. De Pace, and A. Molinari, Phys. Rev. D **72**, 114011 (2005).
[10] A. Mocsy and P. Petreczky, Phys. Rev. D **73**, 074007 (2006).
[11] M. Mannarelli and R. Rapp, Phys. Rev. C **72**, 064905 (2005).
[12] L. Grandchamp, R. Rapp, and G. E. Brown, Phys. Rev. Lett. **92**, 212301 (2004).
[13] L. Grandchamp, S. Lumpkins, D. Sun, H. van Hees, and R. Rapp, Phys. Rev. C **73**, 064906 (2006).
[14] R. Rapp, Eur. Phys. J. A **18**, 459 (2003).
[15] A. Mocsy and P. Petreczky, Eur. Phys. J. C **43**, 77 (2005).
[16] O. Kaczmarek and F. Zantow, Phys. Rev. D **71**, 114510 (2005).
[17] The partial-wave expansion is defined as $T = 4\pi\sum_l(2l+1)T_lP_l(\cos\theta)$, and similarly for the potential.
[18] The on-shell T-matrix is defined for $q = q'$ and $E = \sqrt{s} = 2\omega_q$, with ω_q the (relativistic) on-shell heavy-quark energy.

[19] R. Blankenbecler and R. Sugar, Phys. Rev. **142**, 1051 (1966).
[20] M. I. Haftel and F. Tabakin, Nucl. Phys. **A158**, 1 (1970).
[21] Z. Aouissat, R. Rapp, G. Chanfray, P. Schuck, and J. Wambach, Nucl. Phys. **A581**, 471 (1995).
[22] M. Schmidt, G. Röpke, and H. Schulz, Ann. Phys. (N.Y.) **202**, 57 (1990).
[23] We note that in the calculation of spectral and correlation functions in Sec. IV, the T-matrix (and thus the potential) will only enter fully off-shell and therefore no recourse is taken to any on-shell prescription, cf. Eq. (17).
[24] M. Mannarelli, H. van Hees, and R. Rapp (unpublished).
[25] H. van Hees and R. Rapp, Phys. Rev. C **71**, 034907 (2005).
[26] H. van Hees, V. Greco, and R. Rapp, Phys. Rev. C **73**, 034913 (2006).
[27] S. Digal, P. Petreczky, and H. Satz, Phys. Rev. D **64**, 094015 (2001).
[28] P. Petreczky and K. Petrov, Phys. Rev. D **70**, 054503 (2004); P. Petreczky (private communcation).
[29] O. Kaczmarek and F. Zantow, arXiv:hep-lat/0506019.
[30] C. Y. Wong and H. W. Crater, Phys. Rev. D **75**, 034505 (2007).
[31] H. Satz, arXiv:hep-ph/0602245.
[32] G. S. Bali, H. Neff, T. Duessel, T. Lippert, and K. Schilling (SESAM Collaboration), Phys. Rev. D **71**, 114513 (2005).
[33] G. E. Brown, Philos. Mag. **43**, 467 (1952).
[34] Strictly speaking, $\mathcal{F}(E)$ is not a purely real function since we have included a small imaginary part in the two-particle propagator. More precisely, the bound-state condition, Eq. (7), reads $\mathrm{Re}\{\det\mathcal{F}(E)\} = 0$. We are plotting $\mathrm{Re}\{\det\mathcal{F}(E)\}$ in Figs. 2–4 and 7.
[35] We refer to a ''melting'' or ''dissolving'' state when the scattering amplitude is strongly broadened and diminished corresponding to a loss of the resonant structure.
[36] C. Y. Wong, Phys. Rev. C **76**, 014902 (2007).
[37] F. Karsch, M. G. Mustafa, and M. H. Thoma, Phys. Lett. B **497**, 249 (2001).
[38] W. M. Alberico, A. Beraudo, and A. Molinari, Nucl. Phys. **A750**, 359 (2005).
[39] G. T. Bodwin, E. Braaten, and G. P. Lepage, Phys. Rev. D **51**, 1125 (1995); **55**, 5853(E) (1997).
[40] D. Gromes, Z. Phys. C **26**, 401 (1984).
[41] A. Gara, B. Durand, L. Durand, and L. J. Nickisch, Phys. Rev. D **40**, 843 (1989).
[42] Note that at this level of approximation the distinction between a scalarlike or vectorlike structure for T is immaterial since both have the same heavy-quark limit for the a_l coefficients (modulo global signs).
[43] E. V. Shuryak, Rev. Mod. Phys. **65**, 1 (1993).
[44] R. Rapp, D. Cabrera, and H. van Hees, arXiv:nucl-th/0608033.
[45] D. Cabrera and R. Rapp, Eur. Phys. J. A **31**, 858 (2007).
[46] H. Iida, T. Doi, N. Ishii, H. Suganuma, and K. Tsumura, Phys. Rev. D **74**, 074502 (2006).
[47] T. Umeda, Phys. Rev. D **75**, 094502 (2007).
[48] A. Mocsy and P. Petreczky, arXiv:0705.2559.
[49] W. M. Alberico, A. Beraudo, A. De Pace, and A. Molinari, arXiv:0706.2846.
[50] L. Grandchamp and R. Rapp, Phys. Lett. B **523**, 60 (2001).
[51] R. Machleidt, Adv. Nucl. Phys. **19**, 189 (1989).